Materials Chemistry and Physics 140 (2013) 651–658

Contents lists available at SciVerse ScienceDirect

Materials Chemistry and Physics

journal homepage: www.elsevier.com/locate/matchemphys

Porous media reinforced with carbon soots

Andres E. Fals [a], V.G. Hadjiev [b,c], F.C. Robles Hernández [a,*]

[a] Department of Mechanical Engineering Technology, College of Technology, University of Houston, 304 Technology Building, Houston, TX 77204-4020, USA
[b] Texas Center for Superconductivity, University of Houston, TX 77204-5002, USA
[c] Department of Mechanical Engineering, University of Houston, TX 77204-5002, USA

HIGHLIGHTS

- Alumina porous media can be reinforced with carbon byproducts with controlled porosity.
- Electrical and mechanical properties can be controlled with the amount and type of reinforcement.
- Carbon transformations and processing affect the membrane's properties.
- Permeability, porosity, capillarity, can be controlled with the type of reinforcement.

ARTICLE INFO

Article history:
Received 9 October 2012
Received in revised form
25 March 2013
Accepted 19 April 2013

Keywords:
Ceramics
Microporous materials
Powder metallurgy
Electron microscopy
Electrical properties
Sintering

ABSTRACT

Alumina matrix porous media (composites) can be efficiently reinforced with nanostructured particles of carbon, namely soots. The porous media can be produced a wide range of porosity, conductivity, and hardness. The novelty of this work is the use of carbon byproducts from the synthesis of fullerene and multi walled carbon nanotubes (MWCNT). The soots contain no more than <1 wt% of the pristine quality product. The porous media are manufactured by mechanical milling, sonication, and Spark Plasma Sintering (SPS). Porosity levels between 0% and 28.6% are possible for the fullerene and MWCNT soots respectively. The porosity and permeability depend on the type and amount of carbon additions. The electrical resistivity in the composites was reduced from 7 to 14 orders of magnitude with the hardness ranging from 2 to 19 GPa for membranes reinforced with fullerene or MWCNT soot respectively. The composites are ideal for membrane applications.

Published by Elsevier B.V.

1. Introduction

Porous media have a variety of applications including membranes. The phenomenon of how a fluid is transported in porous media is well known [1,2]. Porous media are commonly used for a variety of uses depending on their densification. Porous membranes are commonly used in liquids separation, while denser membranes are preferred for gases and nanofiltration [3]. A major limitation in the manufacturing of porous media is the industrial repeatability and reproducibility of the products with nanopores [4]. Most of these porous media have been used for membranes that are manufactured by means of: sintering and dip-coating followed by drying and heat processing at different temperatures. Some of the best efforts to produce porous media have resulted in the porous size reduction from 160 nm to 2.5 nm [5–7]. In some cases dip-coating is used to close pores in membranes, the operation is repeated numerous times to reduce defects. More recently, the development of porous media with multifunctionality is well investigated for catalyst and electrochemistry [8]. Porous media are usually manufactured with ceramic using similar procedures as those for composites [9,10]. Reinforcements (e.g. carbon nanostructures) [9–16] are used to improve mechanical properties, hence integrity.

Mechanical milling is selected due to its ability to produce highly homogeneous nanostructured materials, integrity and positive effects on mechanical properties [17,18]. The sonication methods have demonstrated potential in the synthesis of nanostructured materials [19,20]. Sonication is known for its potential to deliver high energy in short periods. Sonication is ideal to break agglomerated particles and to control porosity and homogeneity [21]. Sonication has a positive contribution in increasing the intimacy among the constituents that result in improvements in percolation and density. On the other hand the use of Spark Plasma Sintering (SPS) is proposed to preserve the nanostructure nature of

* Corresponding author. Tel. +1 (713) 743 8231; fax: +1 (505) 213 7106.
E-mail address: fcrobles@uh.edu (F.C. Robles Hernández).

0254-0584/$ – see front matter Published by Elsevier B.V.
http://dx.doi.org/10.1016/j.matchemphys.2013.04.019

the powders during and after processing. The SPS technique had been used not only to sinter, but also to control porosity at low temperatures and short times [9,22–26]. Membranes are design to have multifunctional use such as electronic character, filtration, permeability, coagulation, functionality, osmosis (direct and reverse) and purification among others [15,27,28].

In this work is proposed to reinforce the porous media with carbon nanostructures to improve their mechanical and electrical properties while maintaining their porosity. The proposed methodology guarantees repeatability, reproducibility and consistency of the product. This work describes the methodology to produce homogeneous alumina membranes with multifunctional characteristics. The manufacturing methods include: mechanical milling, sonication and Spark Plasma Sintering (SPS). The characterization conducted in our work includes: Scanning Electron Microscopy (SEM), Transmission Electron Microscopy (TEM), High Resolution Transmission Electron Microscopy (HRTEM), X-ray Diffraction (XRD), and Raman spectroscopy. The reported mechanical and physical properties are: Vickers micro-hardness, density, porosity and electrical resistivity.

2. Materials and methods

Commercial alumina (Al_2O_3) powders (98 wt% purity, mesh 140, particles size $<$ 106 μm) were obtained from Sigma Aldrich. The fullerene soot was purchased from the SESRES Company and has less than 1 wt% of fullerene (C_{60} and C_{70}). The MWCNT soot was donated by the CIMAV-Chihuahua. The MWCNT soot is the raw product of the synthesis containing traces (<1 wt% MWCNT) and the rest is graphite or graphitic carbons and catalyst residue, likely Fe. A throughout characterization of the raw materials is presented in Fig. 1.

Mechanical milling was conducted in a high energy SPEX 8000M on steel hardened mills and milling media. Fullerene soot was milled for 50 h and alumina for 20 h. No mechanical milling was applied to MWCNT; instead, they were only sonicated to prevent mechanical damage to the nanotubes. The milled fullerene soot and alumina powders were milled together for 2 h. After mechanical milling the powders were subjected to sonication. The sonication was conducted in a Misonix 4000 apparatus for 30 min delivering an intensity of 15 j s^{-1} in a powders:ethanol suspension weight ratio of 1:100. Soot additions vary from 1 to 5 wt%. The SPS sintering was conducted on a Dr. Sinter (SPS-515S) system. The SPS conditions were: heating rate of 140 °C s^{-1}, dwelling time of 60 s and temperatures of 1300 °C and 1500 °C. The sintered samples are approximately 12 mm in diameter and 3 mm in thickness. The sintered products were polished following standard metallographic procedures. The polished samples were used for characterization, micro-hardness, electrical properties and density.

X-ray diffraction (XRD) was performed on a D5000 SIEMENS diffractometer equipped with a Cu tube. The characteristic $K_\alpha = 0.15406$ nm operated a 40 kV and 30 A. The SEM observations were carried out on a FEI XL-30FEG on secondary electrons. The TEM/HRTEM was conducted at 200 kV on a JEOL JEM200FXII. The Raman characterization was carried on a Raman XploRA™ Horiba system with a laser line of 532 and 0.5 μm resolution under different grating and collection conditions. Micro-hardness was made on a Future-Tech FX-7 apparatus with 1 kN for 15 s. The reported values are the average of 9 measurements.

The specific gravity was measured based on the Archimedes-spring method with deionized water at standard conditions. The porosity was calculated based on the expressions: $\rho = (m_{Dry} - m_{Wet})/V_{Obj}$ and $P_{Vol} = \rho/m_{Dry}$. Where: ρ is the density, m_{Dry} is the mass of the sample dry, m_{Wet} is the mass of the sample wet, V_{Obj} is the volume of the sample, P_{Vol} is the porosity volume. The wettability and/or permeability analysis was conducted using deionized water and buffer solutions. The deionized water has a pH of 7. Three color buffer solutions were used with pH of 4, 7 and 10 were obtained from EMD Chemicals Inc. Color buffer solutions were selected to assure a constant pH thorough the test. The test was conducted at room temperature under standard atmospheric conditions. The electrical properties were conducted by measuring the resistivity between

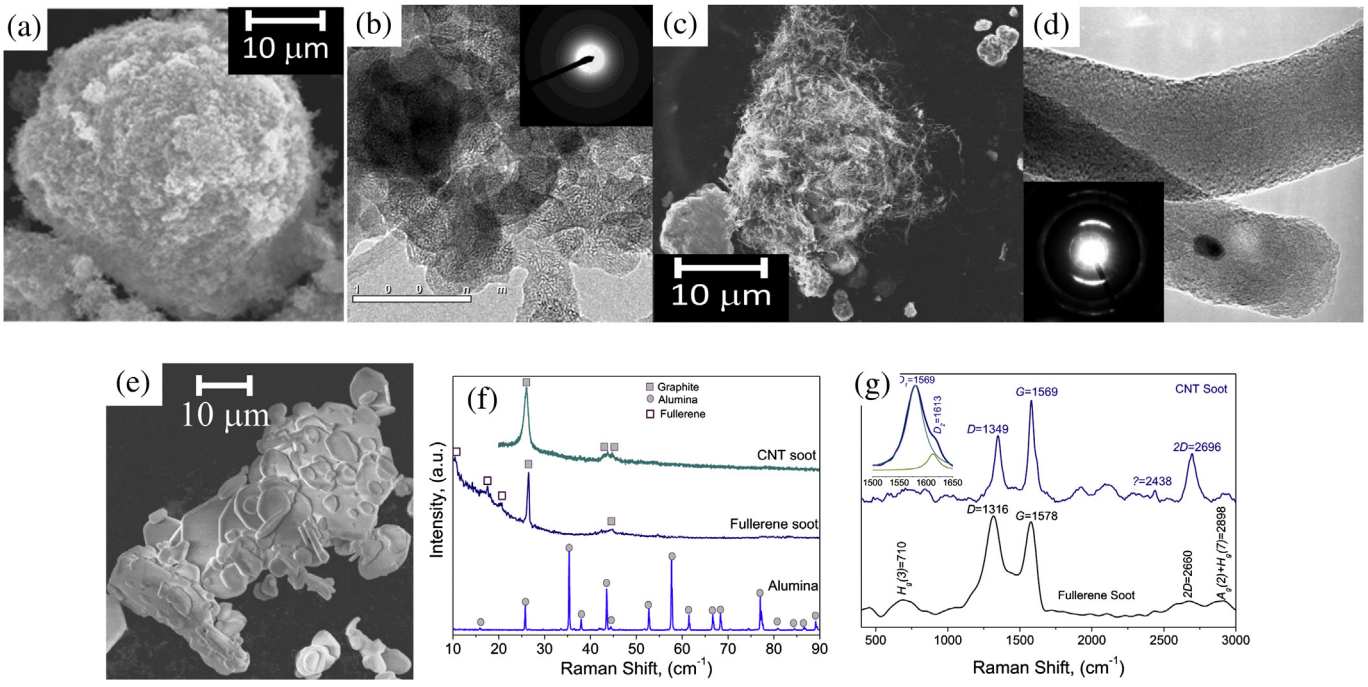

Fig. 1. (a, c, e) Scanning electron micrographs of (a) fullerene, (c) MWCNT soot and (e) raw alumina, (b, d) HRTEM fullerene and MWCNT soot respectively, (f) XRD results of raw materials, (g) Raman of the fullerene and MWCNT soots. The inset in (g) shows a multi-peak *D* band indicating the presence of the MWCNT.

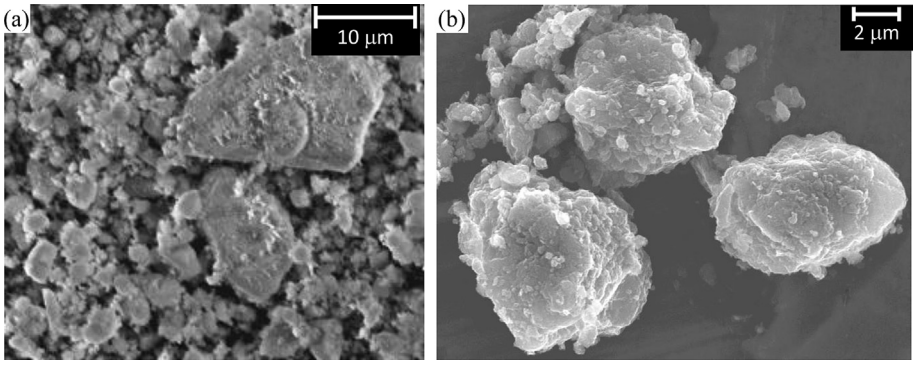

Fig. 2. Scanning electron micrographs for milled powders of (a) Al_2O_3 for 20 h, and (b) fullerene soot SPEX milled for 50 h.

two opposite edges that were polished using a Fluke 8845A Bench Top multimeter with 6 digit precision.

3. Results

3.1. Raw materials

The fullerene soot is characterized for its fluffy appearance (Fig. 1a). The HRTEM images show a quasi-amorphous structure that is further demonstrated by the selected area electron diffraction patter (Fig. 1b). The MWCNT soot is a combination of MWCNT and graphite chunks, Fig. 1c, d presents SEM and HRTEM micrographs and its respective selected area electron diffraction pattern. The XRD in Fig. 1e depicts the crystalline structure of the raw materials in normalized intensity for better visualization. The reflections of the fullerene soot are wider than those on other compounds indicative of smaller grain size corresponding to a disorder structure in a quasi-amorphous stage with traces of fullerene. The ratios among nanotubes and graphite are not as seen in Fig. 1c since MWCNT soot has less than 1 wt% of nanotubes. Fig. 1c, d is presented to depict the presence and characteristics of the nanotubes.

Fig. 1f shows an integrated, over large area, Raman spectrum of the fullerene soot. Characteristic Raman lines and bands of C_{60} and graphitic carbon are clearly discernible in the figure. One fundamental and one second-order combinational Raman lines of C_{60} are identified at 710 cm^{-1} ($H_g(3)$) and at 2898 cm^{-1} ($A_g(2) + H_g(7)$), respectively [29]. The intensity of the other Raman bands of C_{60} is weaker or hidden by more intense bands of the other forms of carbon. The Raman spectrum for the fullerene soot in Fig. 1f is dominated by the *D*, *G* and 2*D* bands of graphitic (sp^2) carbon measured at 1316 cm^{-1}, 1578 cm^{-1}, and 2660 cm^{-1}, respectively. Graphitic carbon may also contribute to the band at 2898 cm^{-1} through the $D + G$ two-phonon scattering channel. Therefore, both Raman and XRD confirm that the fullerene soot contains traces of fullerenes and mostly graphitic carbon. Bases on the suggested algorithms from Ref. [30] the grain size (L_a) in the carbon soot was determined as 40 nm.

Fig. 1g shows the Raman spectrum of the MWCNT soot, generally speaking the *D* (1349 cm^{-1}), *G* (1569 cm^{-1}) and 2*D* (2696 cm^{-1}) bands dominate the spectrum. However the presence of a second band (*D′*) that overlaps with the *G* band. Highly oriented (e.g. single crystal) graphite has an intense *G* band at approximately 1582 cm^{-1} [31, 32]. The *G* band corresponds to the E_{2g} mode that is a first-order scattering. The *D* and *D′* (1613 cm^{-1}) bands are characteristics of sub-micrometric crystals and are directly associated with defects. These bands are assigned to the non-zero phonons [31]. Based on our calculations the L_a in the MWCNT soot is approximately 240 nm. Comparing the *D* bands in both Raman spectrums is clear that the fullerene soot is composed of smaller particles with higher density of defects that is a common characteristic of a quasi-amorphous material.

3.2. Mechanical milling on raw materials

Fig. 2 shows the SEM micrographs of the as milled products after 30 min of sonication. The alumina particles show a refinement and a size distribution when compared to Fig. 1e. The smaller particles and the size distribution are desirable to increase densification within the raw materials for sintering. The milled fullerene soot particles are rather dense and no longer fluffy as the raw product.

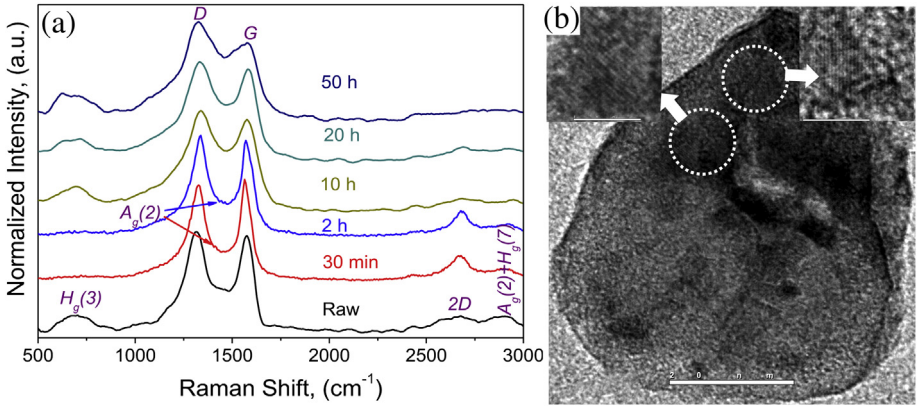

Fig. 3. (a) Raman and (b) HRTEM characterization of fullerene soot. (a) The Raman results represent the as purchased (raw) and SPEX milled samples (0.5–50 h). (b) HRTEM from the SPEX milled product for 50 h, the encircled regions show single nanocrystals of diamond with cubic (Fd3m) structure having a d-spacing (111) = 0.207 nm.

The energy during sonication is enough to break some agglomerates in alumina; however, it may not have the same effect for the larger fullerene soot particles.

Fig. 3 shows the Raman and HRTEM result of the fullerene soot in as purchased (raw) and milled conditions. Fig. 3a is presented in relative intensity. The spectrums of the samples SPEX milled for 0.5 h and 2 h show an increase in the intensity of the 2*D* band. This is attributed to a cold welding/annealing [18] occurring during the mechanical treatment. These two samples show a higher intensity in the *G* band compared to the *D* band. That is tribute to a grain growth resulting from the welding. After 2 h of milling seems that the prevalent mechanism is fracturing resulting in the partial amorphization of the fullerene soot. In the milled fullerene soot the *D* band develops a two-component lineshape with peak intensity shifting from 1318 cm^{-1} in raw soot to 1331 cm^{-1} in soot milled for 20 h (Fig. 3a). The latter is closer to the characteristic Raman frequency of diamond at 1332 cm^{-1} and suggests presence of diamond [33]. The diamond particles are identified by HRTEM in Fig. 3b.

The second-order Raman spectra of 0.5 h and 2 h milled soot are shown in Fig. 3a. Three major bands are clear in both samples. The lowest frequency bands at 2429 cm^{-1} (0.5 h) and 2452 cm^{-1} (2 h) corresponds to $D + D''$ phonon scattering, where D'', typically at ~1100 cm^{-1}, is one of the low frequency defect induced bands in graphite and graphene. The higher frequency of the $D + D''$ band for the 0.5 and 2 h samples is due to the contribution from the second-order band of diamond [34]. The other two bands at 2667–2678 cm^{-1} and 2904–2932 cm^{-1} correspond to Raman scattering involving 2*D* and combinational $D + G$ phonons

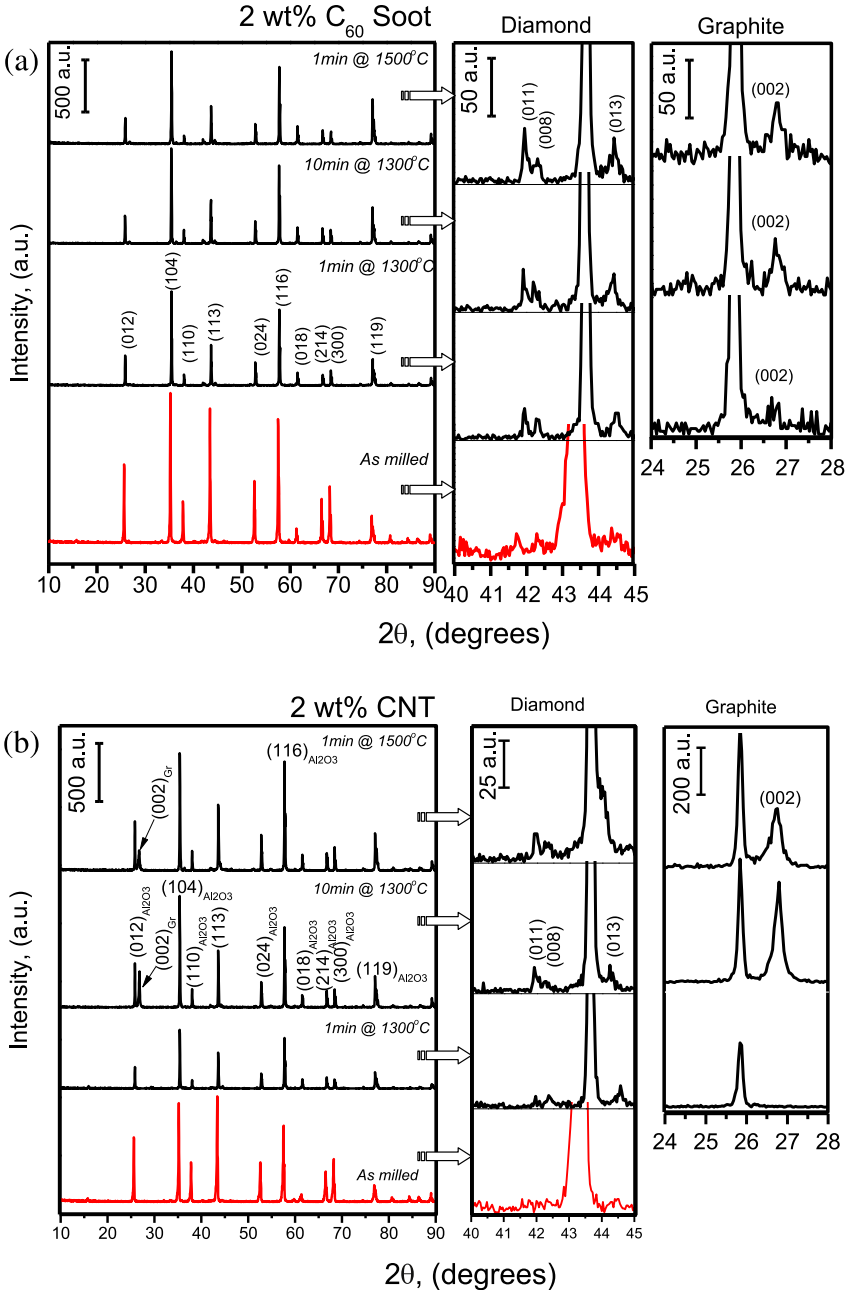

Fig. 4. XRD results for the composites manufactured with (a) fullerene soot and (b) MWCNT soot. The scale in a.u. indicates the equivalency in XRD intensity between spectrums that can be used to relate the relative amount of the respective phase for the various spectrums.

respectively. The intensity of the 2*D* bands in Fig. 3a is surprisingly strong for relatively disordered carbon evidenced by the I_D/I_G ratio. A possible explanation is that among the fractured graphitic particles there is certain amount of graphene, which first-order *D* and *G* bands are hidden by the broad disorder carbon bands. The 2*D* band of graphene is stronger in intensity than its *D* and *G* bands and may dominate the 2*D* spectra. Therefore, we see a strong 2D band in the milled samples indicating the presence of graphene.

Fig. 3b shows HRTEM micrographs where it is identified that milled particles are composed by quasi-amorphous carbon with embedded nanostructured crystals of diamond. Similar findings were previously reported elsewhere for pristine fullerene [35]. The calculated lattice parameters for the identified particles demonstrate that the identified crystals are nanostructured and their respective lattice parameters are: $a_{(\mathrm{Cubic})} = 0.359$ nm, $a_{(\mathrm{Hex})} = 0.255 \pm 0.05$ nm. These lattice parameters correspond to cubic (Fd3m) and hexagonal ($P6_3/mmc$) diamond and have a 0.65% and 1.1% difference with respect to the theoretical values reported in Ref. [36]. Similar results were identified in pure fullerene under milling conditions [37].

3.3. Sintered samples

Fig. 4 presents the XRD results of the sintered alumina membranes reinforced with fullerene or MWCNT soot. The XRD results correspond to the porous media reinforced with 2 wt% C for each soot. The insets in the right side enhance the presence of phases synthesized during milling and SPS. From Fig. 4 is observed that fullerene soot has a tendency to form diamond; while, the MWCNT soot is more effective to synthesize graphite. The SPS conditions (temperature and time) also contribute to the in-situ synthesis of carbon phases. Short times (1 min) and higher temperatures (1500 °C) are effective to transform the fullerene soot into diamond. Longer times (10 min) and lower temperatures are more effective to synthesize graphite and this phenomenon is more evident in the MWCNT soot. The synthesis of diamond is sponsored at higher temperatures for short sintering times. The synthesis of diamond from MWCNT by SPS was previously reported by Zhang et al. [38]; however, the synthesis of diamond by SPS or any other method from fullerene soot has only been reported in Ref. [38].

Fig. 5 shows the results of porosity on each of the composites for the SPS treatments along with representative SEM micrographs. From Fig. 5a is observed that sonication has positive effects on densification. The increase in densification on the sonicated samples is attributed to the breakage of agglomerates in the raw or milled reinforcement that result in improved intimacy among constituents. The SEM micrographs depict the differences in carbon particles present in membranes reinforced with fullerene and MWCNT soot. The sintering mechanisms of the reinforcements are clearly different. The fullerene soot forms a thin layer of carbon coating the alumina particles; such layer builds up during milling. This carbon coating improves toughness, lowering the propensity to fracture as observed in Fig. 5b [39]. The MWCNT particles are chunky and the nanotubes do not guarantee percolation with the matrix.

The electrical resistivity results for both reinforcements are presented in Fig. 6. Pure alumina has a resistivity between 10^{14} and 5×10^{16} Ω cm depending on its purity (from 95 to 99.8 wt%) and testing conditions (air and vacuum) [40]. The porous media presented herein show a resistivity varying from 7.3 ± 1.3 Ω cm to $1.38 \times 10^7 \pm 3 \times 10^6$ Ω cm in atmospheric conditions for the fullerene and MWCNT soot reinforced respectively. The above results represent a reduction in electrical resistant between 7 and 14 orders of magnitude correspondingly. Combining both soots the resistivity decreases to 10^3 Ω cm. Therefore, the fullerene soot has evidently higher contributions to conductivity. The increase of resistivity in the SPS samples at 1300 °C for 10 min is attributed to the graphitization of carbon shorter times have the opposite effect. The 1 wt % of fullerene soot does not have a clear effect on resistivity. Results in Fig. 6b are for the porous media reinforced with MWCNT sonicated for 30 min.

Fig. 7 depicts the differences in wettability and capillarity for the investigated samples. The density results indicate that reinforcements and temperature are the main factor influencing the densification of the membranes. Fullerene soot, short sintering times, high temperature and sonication (30 min) resulted to be the best combination to improve densification. In Fig. 7 is observed that the porous media reinforced with MWCNT have higher capillarity than that observed for the one reinforced with fullerene soot. This is somehow attributed to the difference in zeta potential at a pH of 7 for alumina (~25 mV [41]) and −40 mV in carbon black [42]. Other contributions include the porosity and capillarity. The zeta potential among products is compared to demonstrate that fullerene soot may decrease the permeability. This contribution can be the result of the coating formed along the alumina particles

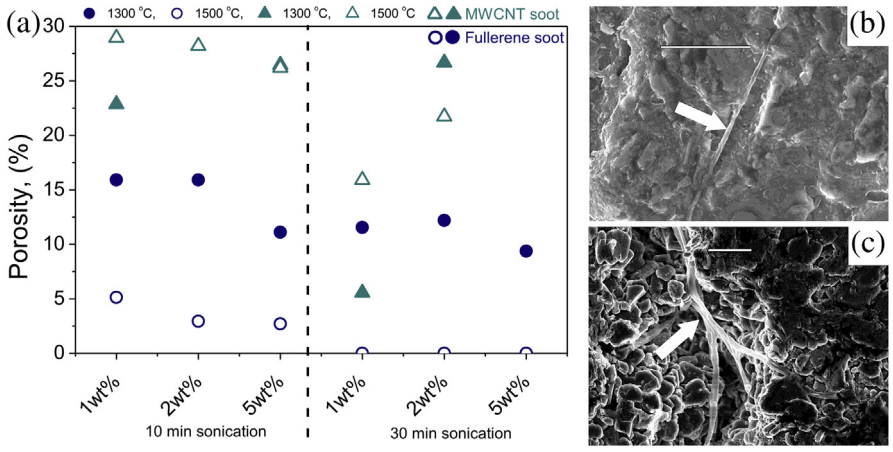

Fig. 5. (a) Porosity analysis for membranes reinforced with MWCNT and fullerene soot, (b, c) SEM micrographs of membranes reinforced with (b) fullerene soot and (c) MWCNT soot, note the relatively large carbon particle. In (b) and (c) are presented zoomed images of nanotubes demonstrating their different integrity with the matrix. The nanotube in (b) was synthesized in situ during SPS. Samples were sonicated for (b) 10 min and (c) 30 min respectively prior to sintering. The carbon coating layer is more evident by comparing (b) with the alumina particles in Figs. 1 and 2.

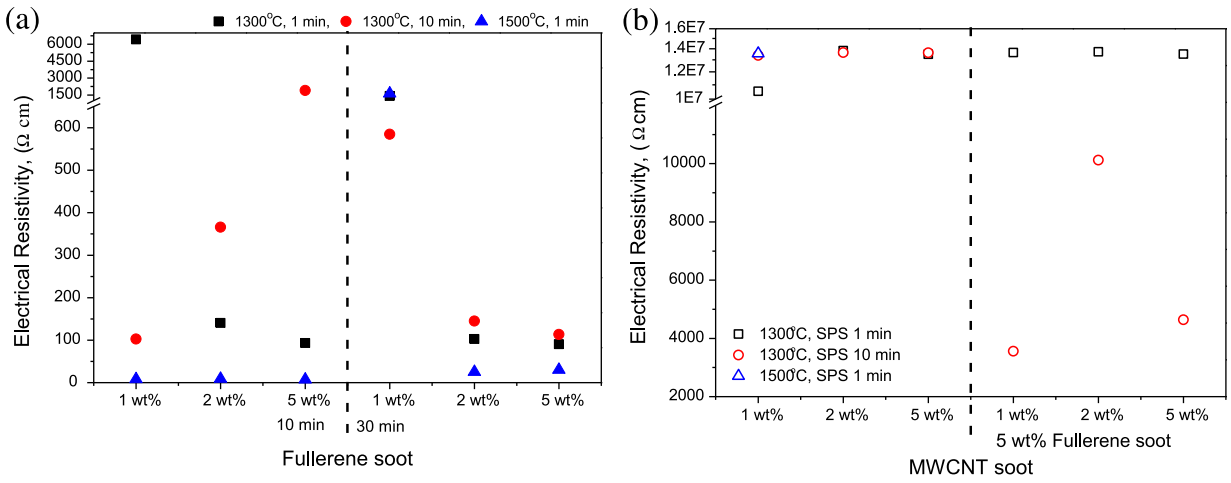

Fig. 6. Electrical conductivity of the sintered samples reinforced with (a) fullerene and (b) MWCNT soot.

(Fig. 7b). The porous media reinforced with MWCNT soot have alumina particles directly exposed, so water can directly wet them (Fig. 7c) decreasing their permeability. The fullerene soot sponsors percolation among the constituent limiting the interaction with water to the surface, which results in improved permeability.

The effect of pH on permeability is demonstrated in Fig. 7. In this figure is shown the higher permeability in the membranes reinforced with fullerene soot. However, for alkaline substances (e.g. pH 11) the permeability of both membranes seems comparable. Also, the permeability of the fullerene soot reinforced composite seems lees permeable in the presence of the acidic buffer (e.g. pH = 4). From the micrographs in Fig. 7 can be observed that the mean pore size is sub-micrometric and nanometric for the samples reinforced with CNT and fullerene soot respectively. The mean porosity determination is ongoing and will be included in future publications.

4. Discussion

The MWCNT soot reinforced samples show lower densification as the sintering temperature densification due to the transformation of the carbon species into graphite (compare Figs. 4 and 5) and compromised percolation. Fullerene soot is more effective to reduce electrical resistivity. Although combining reinforcements is effective; however, large amounts of carbon compromises the membranes' integrity. The 2 wt% of nanostructured carbon additions seem to be the common limit of carbon as reinforcement [9,16,43].

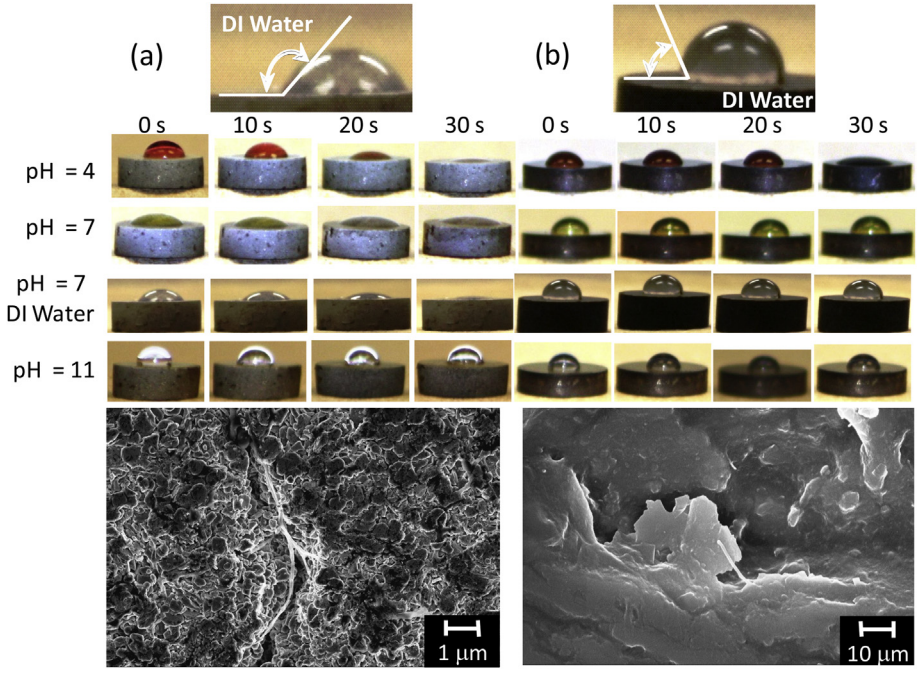

Fig. 7. Examples of the wettability/permeability and pH effect on SPS sintered composites of alumina matrix reinforced with soots: (a) MWCNT or (b) fullerene. Notice the higher capillarity in the MWCNT soot reinforced sample over that on the fullerene soot one as well as the higher permeability for higher pH (pH = 7) as compared to lower pH (pH = 4). DI stands for deionized water.

The importance of the in-situ transformations during SPS is their effect on mechanical and electrical characteristics that can be observed in Figs. 4 and 6. The electrical conductivity of carbon phases vary from 10^{-16} [44,45] to 10^{2} S cm^{-1} [46]. The in-situ synthesis of various carbon phases may contribute to the improved conductivity in the porous media. The characteristics of the porous media presented herein are desirable for membranes for liquid and gases separation in environments where electrochemical character is crucial. The in-situ phase transformations identified in fullerene soot are responsible for their improvements in mechanical and electrical characteristics [39].

The hardness of the porous media varies from 2.45 GPa to 19 GPa depending on the amount and type of soot. The fullerene soot is recommended to preserve the bulk hardness of alumina. Comparing the above hardness with results reported in Ref. [47,48] can be concluded that the materials presented herein have up to 4.3 times higher than the reported alumina. The samples sintered with fullerene soot can preserve the hardness of pure alumina in up to 97% that is the case of highly pure/highly dense alumina [48]. The hardest samples are those reinforced with 1 wt % fullerene soot for 1 min at 1300 °C and 1500 °C. This is attributed to the limited amount of soot; therefore, the testing is conducted almost directly in alumina. However, this practice compromises toughness [39]. On the other end, samples with lower hardness are those reinforced with MWCNT soot that is the most porous (Fig. 5).

The processing methodology has a direct influence on the physical and mechanical characteristics of the manufactured samples. Surprisingly, sonication time is a key contributor to porosity and resistivity. There is a correlation among sonication, SPS time, temperature and reinforcement with resistivity. In general 1300 °C and 1 wt% of fullerene soot doesn't seem to be as effective to reduce resistivity as larger additions or higher temperature (1500 °C). The fullerene soot additions are more effective to reduce the resistivity than MWCNT soot. The combination of fullerene and MWCNT soot is effective to reduce resistivity but only to intermediate values between reinforcements.

MWCNT soot is an ideal reinforcement to produce porous media or membranes due to poor percolation with alumina. On the other hand fullerene soot reduces capillarity by creating a thin film along the alumina particles and prevents porosity due to a better percolation with alumina. Due to the hydrophobicity of carbon (Z potential) the fullerene soot increases the membrane's permeability (Fig. 7a) reducing its wettablity. However, this is clearly affected by the environment at which the membranes are exposed, since acid or basic environments clearly affect their capillarity. Alumina is more hydroscopic and permits a relatively easier water transfer in neutral or basic pH environments. In this work is demonstrated that carbon byproducts (soots) have comparable effects to produce porous media as the pristine quality carbon molecules (nanotubes, fullerenes, graphene, etc.).

5. Conclusions

The porous media presented herein is ideal for applications such as membranes where electrochemical characteristics are desirable. Sonication has positive effects on porosity, density and resistivity. The fullerene soot and processing methods are ideal to coat the alumina particles resulting in improved characteristics of the sintered products. The carbon in the fullerene soot has the tendency to transform into diamond during milling and SPS. On the contrary, the MWCNT soot has a higher tendency to transform into graphite. The permeability, electrical conductivity, density and hardness are improved with fullerene soot. The MWCNT soot enhances porosity and capillarity. Capillarity increases with low pH and decreases with higher pH; though, the fullerene soot membranes are more permeable pH.

Acknowledgments

FCRH would like to express his gratitude to the University of Houston and the Government of Texas for the Start Up and HEAFS funding. The authors would like to thank Dr. D. Butt for facilitating the Spark Plasma Sintering facilities at Center for the Advanced of Energy Studies (CAES) at Idaho Falls. We want to express our gratitude to Dr. G. Majkic at the Mechanical Engineering Department (University of Houston) for supporting this work with the micro-hardness testing and equipment.

References

[1] J.L. Vazquez, The Porous Medium Equation: Mathematical Theory, Oxford University Press, Oxford, 2006.
[2] J.L. Vazquez, The Porous Medium Equation: Mathematical Theory, Clarendon, Oxford, 2007.
[3] R.M. de Vos, H. Verweij, Science 279 (1998) 1710–1711.
[4] D.E. Fain, G.E. Roettger, Abstr. Pap. Am. Chem. Soc. 210 (1995) 44.
[5] R.J.R. Uhlhorn, K. Keizer, A.J. Burggraaf, J. Memb. Sci. 66 (1992) 259–269.
[6] R.J.R. Uhlhorn, K. Keizer, A.J. Burggraaf, J. Memb. Sci. 66 (1992) 271–287.
[7] R.J.R. Uhlhorn, M.H.B.J.H. Intveld, K. Keizer, A.J. Burggraaf, J. Mater. Sci. 27 (1992) 527–537.
[8] M. Roso, S. Sundarrajan, D. Pliszka, S. Ramakrishna, M. Modesti, Nanotechnology 19 (2008).
[9] F.C. Robles-Hernandez, H.A. Calderon, Jom-Us 62 (2010) 63–68.
[10] V. Garibay-Febles, H.A. Calderon, F.C. Robles-Hernadez, M. Umemoto, K. Masuyama, J.G. Cabanas-Moreno, Mater. Manuf. Process 15 (2000) 547–567.
[11] G.D. Zhan, J. Kuntz, J. Wan, J. Garay, A.K. Mukherjee, J. Am. Ceram. Soc. 86 (2003) 200–202.
[12] G.D. Zhan, J. Kuntz, J. Wan, J. Garay, A.K. Mukherjee, Scripta Mater. 47 (2002) 737–741.
[13] E. Zapata-Solvas, D. Gomez-Garcia, R. Poyato, Z. Lee, M. Castillo-Rodriguez, A. Dominguez-Rodriguez, V. Radmilovic, N.P. Padture, J. Am. Ceram. Soc. 93 (2010) 2042–2047.
[14] G.D. Zhan, J.D. Kuntz, J.E. Garay, A.K. Mukherjee, Appl. Phys. Lett. 83 (2003) 1228–1230.
[15] E.S. Kim, G. Hwang, M.G. El-Din, Y. Liu, J. Memb. Sci. 394 (2012) 37–48.
[16] F.C. Robles Hernández, H.A. Calderon, Mater. Chem. Phys. 132 (2012) 815–822.
[17] P.S. Gilman, J.S. Benjamin, Annu. Rev. Mater. Sci. 13 (1983) 279–300.
[18] C. Suryanarayana, Prog. Mater. Sci. 46 (2001) 1–184.
[19] L. Gonzalez-Reyes, I. Hernandez-Perez, F.C.R. Hernandez, H.D. Rosales, E.M. Arce-Estrada, J. Eur. Ceram. Soc. 28 (2008) 1585–1594.
[20] F.C. Robles Hernandez, L. Gonzalez-Reyes, I. Hernandez-Perez, Chem. Eng. Sci. 66 (2011) 721–728.
[21] T. Chave, S.I. Nikitenko, D. Granier, T. Zemb, Ultrason. Sonochem. 16 (2009) 481–487.
[22] F.C. Robles-Hernández, Improvement in Functional Characteristics of Al–Si Cast Components through the Utilization of a Novel Electromagnetic Treatment of Liquid Melts, Mechanical Engineering, University of Windsor, Windsor, ON Canada, 2004, p. 251.
[23] F.C. Robles-Hernández, Production and Characterization of (Al, Fe)–C (Graphite or Fullerene) Composites Prepared by Mechanical Alloying, Metallurgy, Materials Science and Engineering, Instituto Politécnico Nacionál, Mexico City, Mexico, 1999, p. 150.
[24] A.E. Fals, J. Quintero, F.C.R. Hernández, MRS Symp. Proc. 1276 (2010) 21–30.
[25] N. Chennoufi, G. Majkic, Y.C. Chen, K. Salama, Metall. Mater. Trans. A 40A (2009) 2401–2409.
[26] G. Maikic, S. Karajagi, U. Balachandran, K. Salama, Mat. Sci Eng B-Solid 150 (2008) 145–150.
[27] K.P. Lee, T.C. Arnot, D. Mattia, J. Memb. Sci. 370 (2011) 1–22.
[28] J. Caro, M. Noack, Microporous Mesoporous Mater. 115 (2008) 215–233.
[29] Z.H. Dong, P. Zhou, J.M. Holden, P.C. Eklund, M.S. Dresselhaus, G. Dresselhaus, Phys. Rev. B 48 (1993) 2862–2865.
[30] L.G. Cancado, K. Takai, T. Enoki, M. Endo, Y.A. Kim, H. Mizusaki, A. Jorio, L.N. Coelho, R. Magalhaes-Paniago, M.A. Pimenta, Appl. Phys. Lett. 88 (2006).
[31] L. Nikiel, P.W. Jagodzinski, Carbon 31 (1993) 1313–1317.
[32] P. Lespade, R. Al-Jishi, M.S. Dresselhaus, Carbon 20 (1982) 427–431.
[33] S. Prawer, R.J. Nemanich, Philos. Trans. R. Soc. A 362 (2004) 2537–2565.
[34] S.A. Solin, A.K. Ramdas, Phys. Rev. B 1 (1970) 1687–1698.
[35] I. Santana-García, F. Hernandez-Robles, V. Garibay-Febles, H. Calderon, Microsc. Microanal. 16 (2010) 1688–1689.
[36] P. Darrell Ownby, X. Yang, J. Liu, J. Am. Ceram. Soc. 75 (1992) 8.

[37] I.I. Santana, F.C. Robles Hernandez, V.Garibay Febles, H.A. Calderon, Solid State Phenom. 172–174 (2011) 727–732.
[38] F.M. Zhang, J. Shen, J.F. Sun, Y.Q. Zhu, G. Wang, G. McCartney, Carbon 43 (2005) 1254–1258.
[39] A.E. Fals, V.G. Hadjiev, F.C. Robles Hernández, Mater. Sci. Eng. A 558 (2012) 13–20.
[40] Y. Yamano, T. Komiyama, M. Takahashi, S. Kobayashi, K. Nitta, Y. Saito, Proc. ISDEIV (2008) 35–38.
[41] T. Gopal, J.B. Talbot, J. Electrochem. Soc. 153 (2006) G622–G625.
[42] H. Sis, M. Birinci, Colloid Surf. A 341 (2009) 60–67.
[43] K. Ahmad, W. Pan, S.L. Shi, Appl. Phys. Lett. 89 (2006).
[44] J.H. Du, L. Zhao, Y. Zeng, L.L. Zhang, F. Li, P.F. Liu, C. Liu, Carbon 49 (2011) 1094–1100.
[45] M.H. Miao, Carbon 49 (2011) 3755–3761.
[46] L. Kumari, V. Prasad, S.V. Subramanyam, Carbon 41 (2003) 1841–1846.
[47] Z. Xia, L. Riester, B.W. Sheldon, W.A. Curtin, J. Liang, A. Yin, J.M. Xu, Rev. Adv. Mater. Sci. 6 (2004) 131–139.
[48] A. Krell, P. Blank, J. Am. Ceram. Soc. 78 (1995) 1118–1120.